Molecular Cell, Vol. 8, 829–839, October, 2001, Copyright ©2001 by Cell Press

The Crystal Structure of the PX Domain from p40^{phox} Bound to Phosphatidylinositol 3-Phosphate

Jerónimo Bravo,[1,4] Dimitrios Karathanassis,[1,4] Christine M. Pacold,[1,4] Michael E. Pacold,[1,4] Chris D. Ellson,[2] Karen E. Anderson,[2] P. Jonathan G. Butler,[1] Isabelle Lavenir,[1] Olga Perisic,[1] Phillip T. Hawkins,[2] Len Stephens,[2] and Roger L. Williams[1,3]

[1] Medical Research Council
Laboratory of Molecular Biology
Hills Road
Cambridge CB2 2QH
United Kingdom

[2] The Inositide Laboratory
The Babraham Institute
Babraham
Cambridge CB2 4AT
United Kingdom

Summary

More than 50 human proteins with a wide range of functions have a 120 residue phosphoinositide binding module known as the PX domain. The 1.7 Å X-ray crystal structure of the PX domain from the p40^{phox} subunit of NADPH oxidase bound to PtdIns(3)P shows that the PX domain embraces the 3-phosphate on one side of a water-filled, positively charged pocket and reveals how 3-phosphoinositide specificity is achieved. A chronic granulomatous disease (CGD)-associated mutation in the p47^{phox} PX domain that abrogates PtdIns(3)P binding maps to a conserved Arg that does not directly interact with the phosphoinositide but instead appears to stabilize a critical lipid binding loop. The SH3 domain present in the full-length protein does not affect soluble PtdIns(3)P binding to the p40^{phox} PX domain.

Introduction

The phox homology (PX) domain was first identified in the p40^{phox} and p47^{phox} subunits of NADPH oxidase (Ponting, 1996). In addition to NADPH oxidase, PX domains are found in class II phosphoinositide 3-kinases (PI3Ks), sorting nexins (SNX), yeast Vps proteins, bud emergence proteins (Bem), mammalian phospholipase D (PLD), cytokine-independent survival kinase (CISK), and SNAREs (e.g., Vam7). Originally, it was suggested that PX domains might bind SH3 domains. Indeed, a recent NMR study of the PX domain from p47^{phox} revealed that a conserved proline-rich motif in this domain acts as the ligand for the C-terminal SH3 domain from the same protein (Hiroaki et al., 2001). Moreover, several recent reports demonstrate that a variety of PX domains can also serve as phosphoinositide binding modules (reviewed in Prehoda and Lim, 2001; Simonsen and Stenmark, 2001; Wishart et al., 2001). The PX domains of Vam7 (Cheever et al., 2001), SNX3 (Xu et al., 2001b), and p40^{phox} (Ellson et al., 2001b; Kanai et al., 2001) specifically bind to phosphatidylinositol-3-phosphate (PtdIns(3)P), while the PX domains of p47^{phox} and PI3K-C2α bind preferentially to phosphatidylinositol-3,4-bisphosphate (PtdIns(3,4)P_2) and PtdIns(4,5)P_2, respectively (Kanai et al., 2001; Song et al., 2001). Binding of PtdIns(3)P by intact p40^{phox} stimulates NADPH oxidase activity (Ellson et al., 2001b).

The NADPH oxidase in phagocytic cells such as neutrophils and macrophages is a key component of innate immunity that is activated upon phagocytosis of foreign particles. The primary product of the reaction catalyzed by NADPH oxidase is superoxide (O_2^-) that in turn generates microbicidal reactive oxygen species (ROS) in the phagocytic vesicles. The NADPH oxidase is composed of a membrane-bound, catalytic gp91^{phox}/p22^{phox} heterodimer known as flavocytochrome b_{558} and of a cytosolic regulatory complex consisting of p40^{phox}, p47^{phox}, p67^{phox}, and Rac. In resting neutrophils, the oxidase is inactive. Upon stimulation of the cells, the regulatory complex translocates to the plasma membrane where it activates the catalytic machinery (Segal and Abo, 1993; Babior, 1999). Naturally occurring mutations in gp91^{phox}, p47^{phox}, and p67^{phox} are associated with a severe susceptibility to infection known as chronic granulomatous disease (CGD). It has been long recognized that PI3K plays a vital role in activation of NADPH oxidase and phagocytosis (Baggiolini et al., 1987; Arcaro and Wymann, 1993; Okada et al., 1994; Cox et al., 1999); however, the molecular mechanism for this has remained unclear. Recent findings that the PX domains from p40^{phox} and p47^{phox} bind to the lipid products of PI3K are beginning to clarify the role of PI3K in ROS formation (Ellson et al., 2001b; Kanai et al., 2001). An accumulation of PtdIns(3,4,5)P_3 occurs at the site of the developing phagocytic cup when opsonized particles are phagocytosed by RAW 264.7 macrophages (Marshall et al., 2001). Following sealing of the phagosomal vacuole, there is a rapid increase in PtdIns(3)P on the surface of the internalized phagosome as indicated by accumulation of GFP-tagged p40^{phox} PX domains and FYVE domains (another type of PtdIns(3)P binding module) (Ellson et al., 2001a). The rapid appearance of PtdIns(3)P in phagosomal membranes is consistent with an earlier observation that the FYVE domain-containing protein EEA1 can be found associated with phagosomes (Scianimanico et al., 1999).

To gain insight into the membrane targeting mechanism of PX domains, we have determined the 1.7 Å X-ray crystal structure of the PX domain from p40^{phox} bound to soluble di-butanoyl-PtdIns(3)P.

Results and Discussion

Overall Structure of the p40^{phox} PX Domain

The construct used for the structure determination consists of p40^{phox} residues 2–149 encompassing the PX domain (residues 16–134) and N- and C-terminal helical

[3] Correspondence: rlw@mrc-lmb.cam.ac.uk

[4] These authors contributed equally to this work.

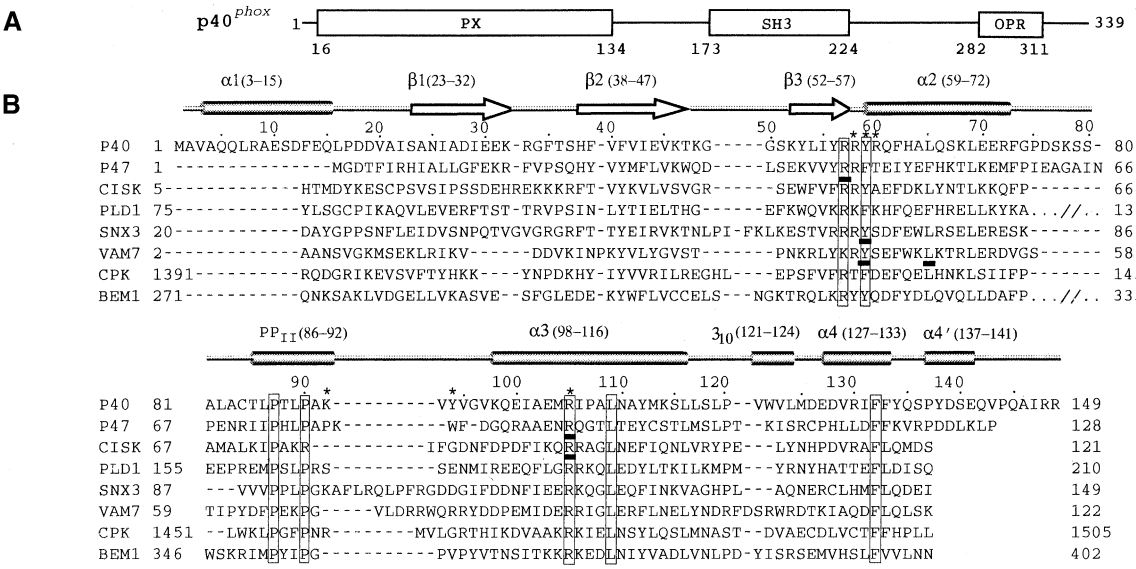

Figure 1. Domain Structure of the Human p40*phox* Protein and Sequence Alignment of the PX Domains

(A) Schematic drawing of the human p40*phox* protein, indicating the location of the PX domain, the Src homology 3 (SH3) domain, and the octicosapeptide repeat (OPR).

(B) Secondary structure-based sequence alignment of eight representative PX domains, obtained from the Conserved Domain Database (NCBI) and manually adjusted. Residues in boxes are conserved. Residues having side chains interacting with PtdIns(3)P are indicated by asterisks. Underlined residues indicate previously characterized mutations in PX domains: mutation R42Q in p47*phox* has been identified in a subset of CGD patients (Noack et al., 2001) and eliminates phosphoinositide binding (Kanai et al., 2001). Mutation R90L in p47*phox* reduces lipid binding (Kanai et al., 2001) and in CISK abolishes endosomal localization (Xu et al., 2001a). Mutations Y71A in SNX3 (Xu et al., 2001b) and Y42A and L48Q in Vam7 (Cheever et al., 2001) compromise the PX domain function.

extensions (Figure 1). The N-terminal residues preceding the PX domain of p40*phox* (helix α1) were essential for obtaining soluble expression of the isolated PX domain. The structure reveals that helix α1 covers a fairly extensive hydrophobic patch consisting of Val20, Ile22, Val121, Leu124, and Met125. The PX domain has a wedge-like overall shape with maximal dimensions of 50 Å × 40 Å × 20 Å and two fairly flat faces (Figure 2). The thinner of these two faces has a cluster of basic residues lining a pocket that binds the PtdIns(3)P (Figure 3).

The fold of the p40*phox* PX domain is similar to the NMR structure of the p47*phox* PX domain (Hiroaki et al., 2001). The PX domain fold has an N-terminal three-stranded, meander topology β sheet packed against a helical subdomain beginning at residue 59 that consists of four α helices, a 3_{10} helix, and a type II polyproline helix (Figure 2). Strand β1 has a β bulge at residues 27–28 (also conserved in p47*phox*, residues 12–13) that twists the β sheet toward the phosphoinositide binding site so that the edge of the N-terminal end of strand

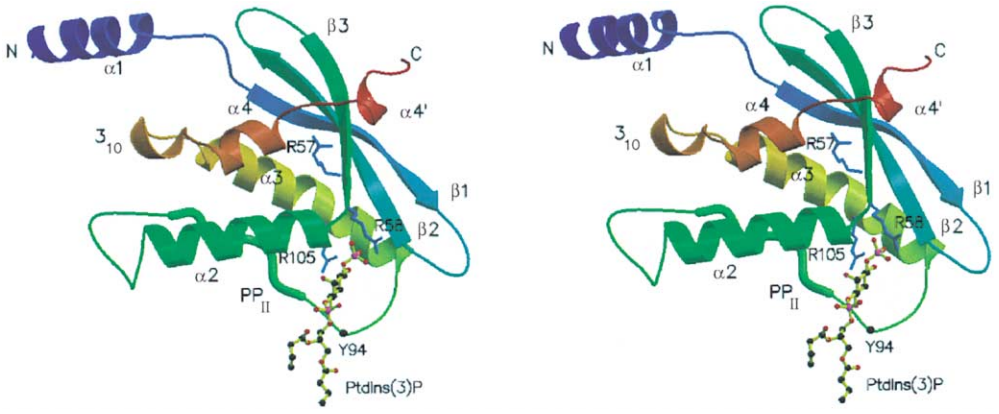

Figure 2. Stereo Ribbon Diagram of the p40*phox* PX Domain

The protein is colored from blue at the N terminus to red at the C terminus, and the bonds of the di-C4-PtdIns(3)P are colored yellow. The secondary structure elements, including the polyproline helix (PP_{II}), are labeled. Arg57, Arg58, and Arg105, which are highly conserved in PX domains, are rendered as cyan sticks. The position of the diacylglycerol-interacting residue Tyr94 is marked with a sphere. Unless otherwise indicated, figures were prepared with MOLSCRIPT (Kraulis, 1991) and RASTER3D (Merritt and Bacon, 1997).

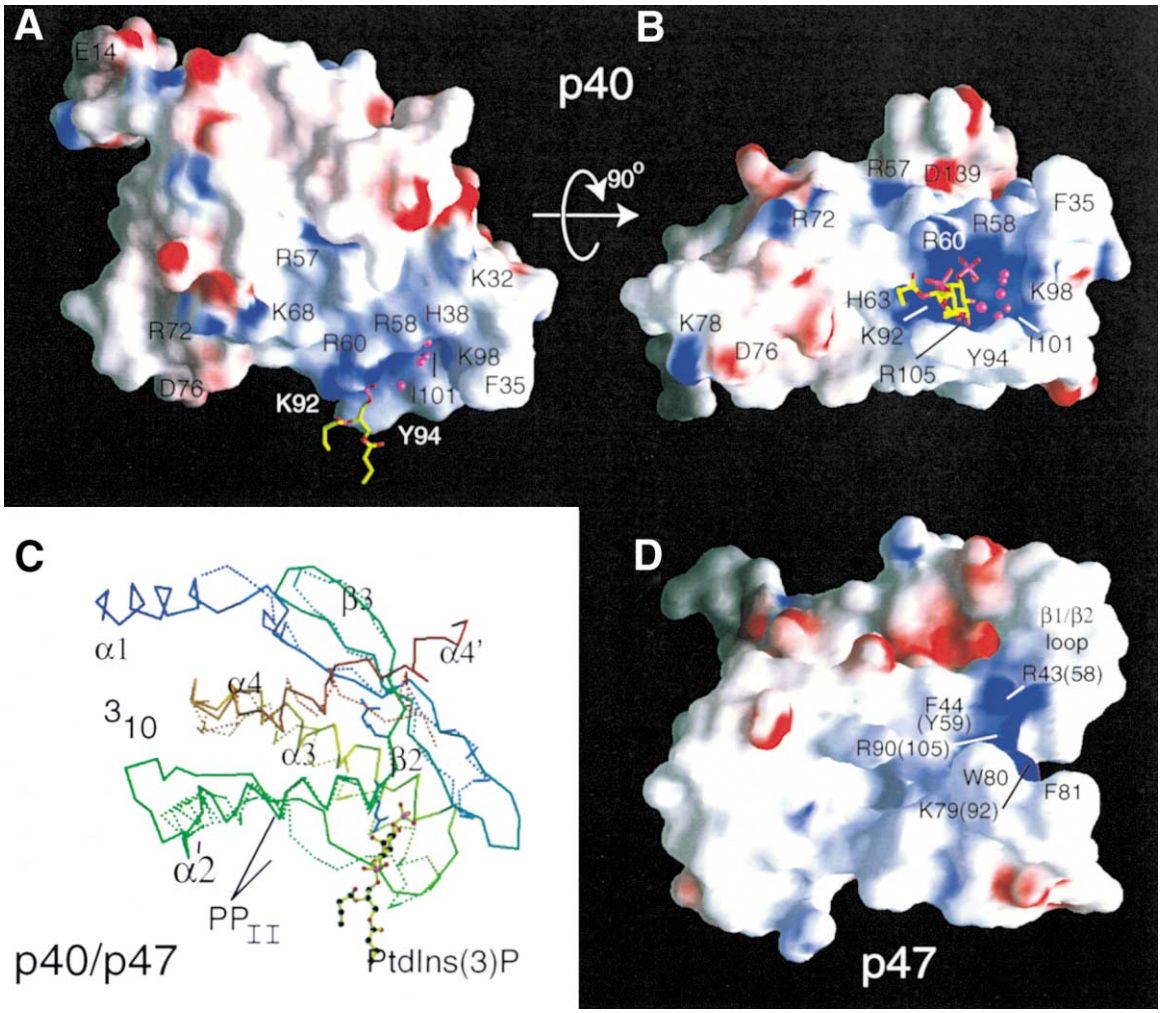

Figure 3. Surface Representations of the p40^{phox} PX Domain Bound to di-C4-PtdIns(3)P and Comparison with the p47^{phox} PX Domain

(A) Side view of the p40^{phox} PX domain colored by electrostatic potential. Negatively charged regions are shown in red and positively charged in blue (ranging from −18 kT/e$^-$ to 24 kT/e$^-$). The lipid is drawn as sticks, and waters occupying the headgroup binding pocket are colored magenta. Surface representations were prepared with GRASP (Nicholls et al., 1991).

(B) View from the membrane of the p40^{phox} PX domain, colored by potential.

(C) Cα traces of the overall structures of the p40^{phox} and p47^{phox} PX domains. The representative conformation from the NMR structure of the p47^{phox} PX domain (PDB entry 1GD5) (Hiroaki et al., 2001) is shown as dotted lines superimposed on the crystal structure of the p40^{phox} PX domain (solid lines). The traces are colored from blue at the N terminus to red at the C terminus.

(D) View from the membrane of the p47^{phox} PX domain conformer number 7 from the NMR structure (with binding pocket most similar to the p40^{phox} PX/PtdIns(3)P complex), colored by potential. Several residues of p47^{phox} are labeled, with the p40^{phox} equivalent numbers in parentheses.

β_2 forms one wall of the binding pocket. The principal structural differences between the p47^{phox} and p40^{phox} PX domains occur in the portion of the helical subdomain C-terminal to helix α2, particularly the PP$_{II}$ helix and the portion of the PtdIns(3)P pocket that immediately follows PP$_{II}$ (Figure 3).

Structure of the Phosphoinositide Binding Pocket

As determined by isothermal titration calorimetry, di-C4-PtdIns(3)P binds the PX domain with a K_d of 5 μM (Figure 4). Both the headgroup and diacylglycerol moiety of the bound PtdIns(3)P are well defined in the electron density (Figure 5). The phosphoinositide headgroup occupies one corner of a pocket that is about 7 Å deep with an external opening of about 10 Å × 8 Å (Figure 3). The remainder of the pocket is filled with well-ordered water molecules. Residues from three regions, the β3/α2 loop, the PP$_{II}$/α3 loop, and the N-terminal halves of strand β2 and helix α3 build the walls of the pocket. Conserved residues from these three regions interact with the 3-phosphate, 1-phosphate, and 4/5-hydroxyl of the PtdIns(3)P, respectively. Tyr59, a conserved residue from the β3/α2 loop, forms the floor of the binding pocket.

Determinants of PtdIns(3)P Specificity

The 3-Phosphate Interactions

Arg58, a residue within the conserved β3/α2 loop that connects the β sheet to the helical subdomain, forms the most extensive interactions with the 3-phosphate

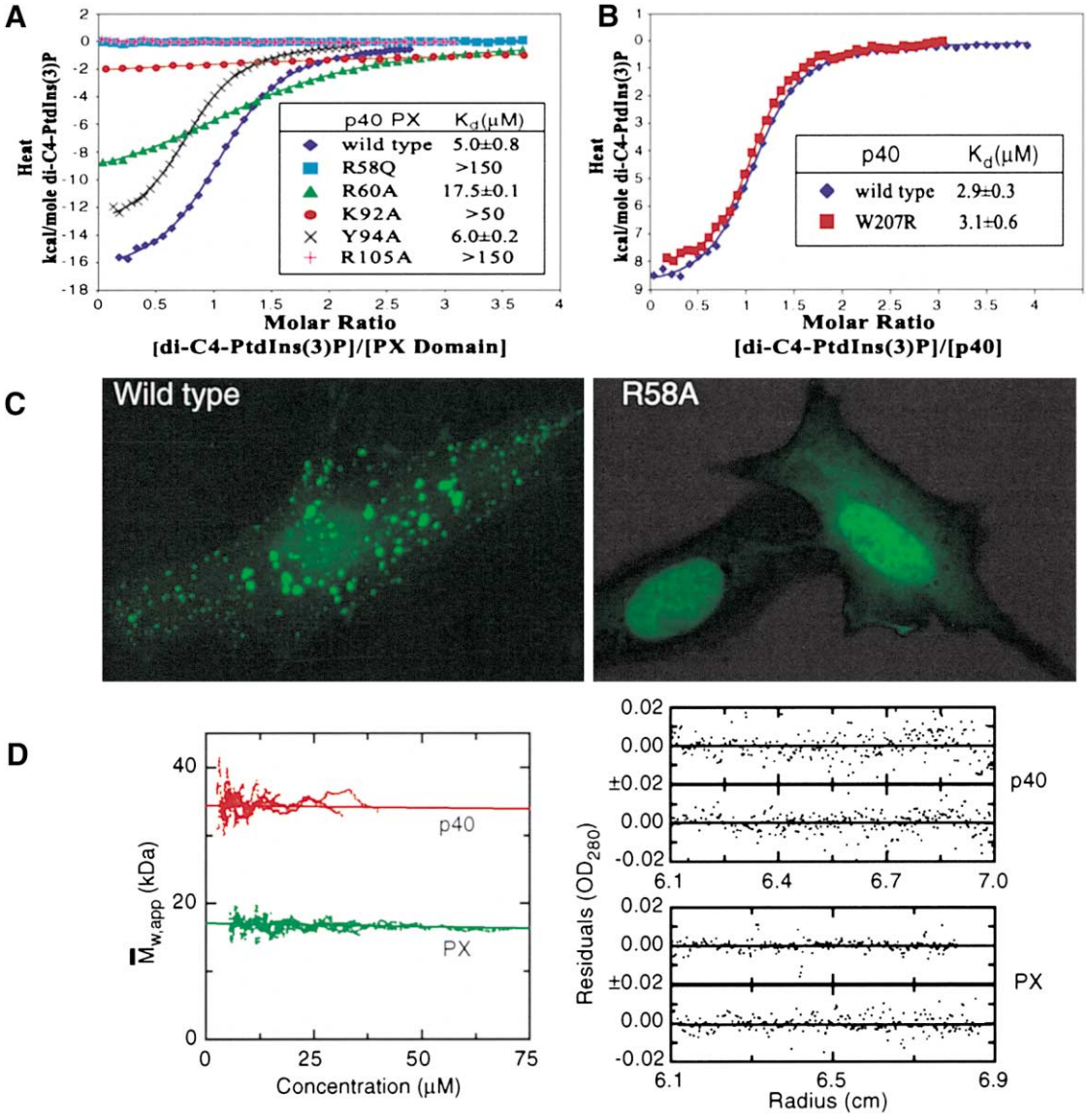

Figure 4. PtdIns(3)P Binding to the Monomeric Isolated p40^{phox} PX Domain and Full-Length p40^{phox}

(A) Isothermal titration calorimetry profiles for the binding of di-C4-PtdIns(3)P to wild-type and mutant p40^{phox} PX domains. The fits to the data are shown as solid lines. The mean K_ds and their standard deviations were calculated from two to five measurements for each protein.
(B) Isothermal titration calorimetry profiles for the binding of di-C4-PtdIns(3)P to wild-type and W207R mutant full-length p40^{phox}.
(C) Subcellular distribution of wild-type GFP-p40^{phox} PX (left) and R58A mutant p40^{phox} PX (right) in PAE cells. PAE cells were transiently transfected with DNA encoding GFP fusion proteins of the isolated PX domain of p40^{phox}, either wild-type (WT) or R58A mutant.
(D) Analytical ultracentrifugation of the p40^{phox} PX domain and the full-length protein. Plots of apparent, weight-average molecular mass ($M_{w,app}$) against concentration for full-length p40^{phox} and the p40^{phox} PX domain are shown on the left. Data are from multiple cells in different centrifuge runs, with the full-length protein shown in red and the PX domain in green. Plots of the fitting residuals for two cells of each protein (right), show the good fit of the model. The apparent M_1 and B values from these fits were used to draw lines on the $M_{w,app}$ against concentration plots. The analysis yields estimated masses of 34,400 Da and 17,100 Da for the full-length and PX domains, respectively. These masses agree well with the monomeric masses calculated from the sequence (39,926 Da and 17,944 Da, respectively).

of the bound PtdIns(3)P. Oxygens of the 3-phosphate form hydrogen bonds with NH2 and NE in the side chain of Arg58. In p40^{phox}, Arg58 is critical for PtdIns(3)P binding. When it is mutated to Gln, PtdIns(3)P binding in vitro is lost (Figure 4), although circular dichroism (CD) spectroscopy indicates that the mutation has no effect on the overall fold of the protein (data not shown). Mutation of the same residue eliminates the distinct punctate pattern characteristic of the p40^{phox} PX domain endosomal localization in vivo (Figure 4). The essential role of a basic residue at a position equivalent to Arg58 in 3-phosphate binding by PX domains has been obscured in previous studies because it was mutated only in conjunction with two other residues that have critical but different functions (triple mutation of the entire RRY motif in the β3/α2 loop, 57–59 in p40^{phox}) (Xu et al., 2001b).

A basic residue analogous to R58 of p40^{phox} is conserved in most PX domains (77% of those in the Pfam

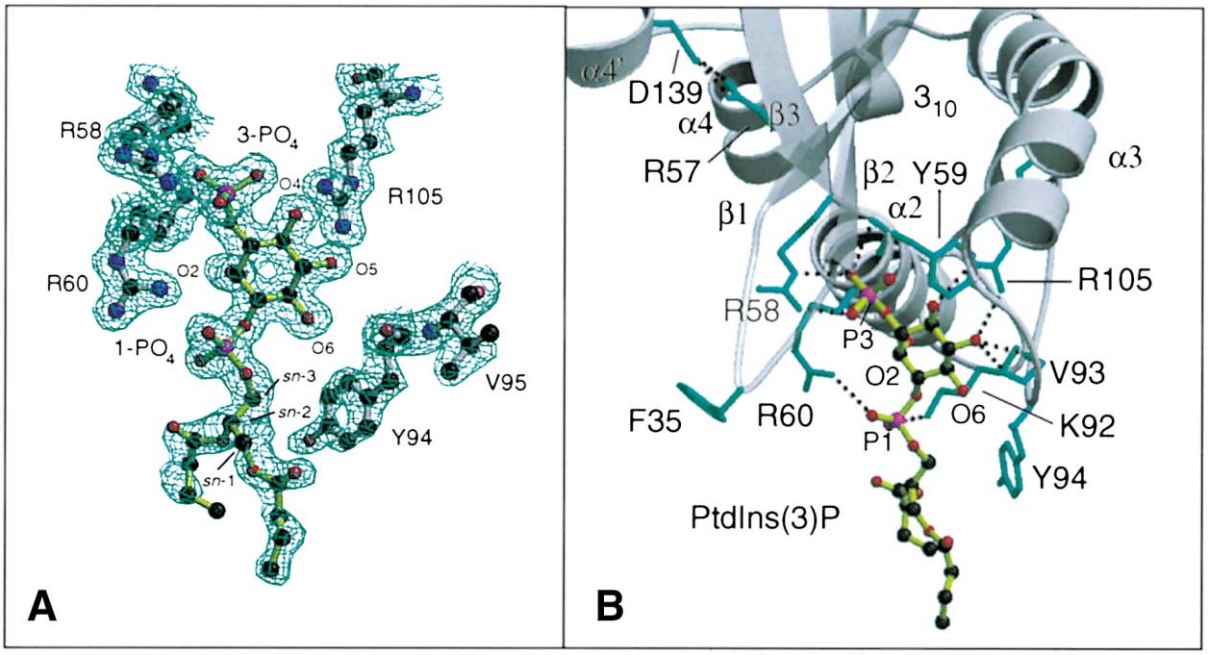

Figure 5. PtdIns(3)P Bound to the p40^{phox} PX Domain

(A) σ_A-weighted electron density for the di-C4-PtdIns(3)P and some of the surrounding amino acids. The $2mF_o$-DF_c map was contoured at 1 σ and rendered with BOBSCRIPT (Esnouf, 1999).

(B) A view of the PtdIns(3)P binding pocket. Interacting residues are drawn as cyan sticks, and hydrogen bonds are shown by dashed lines. The inositol ring also makes hydrophobic contacts with the side chain of Tyr59, and the diacylglycerol moiety makes hydrophobic contacts with the side chain of Tyr94. In addition, the Arg57/Asp139 salt link is shown.

[Bateman et al., 2000] seed alignment). An equivalent basic residue is present in all of the PX domains that have been reported to bind 3-phosphoinositides, including SNX3, SNX7, SNX16, Vam7, CISK, and p47^{phox} PX domains (Cheever et al., 2001; Kanai et al., 2001; Xu et al., 2001a, 2001b). In contrast, there is no basic residue analogous to Arg58 in a small subset of PX domains, e.g., the PX domains of class II PI3Ks. Consistent with this, the PX domain of PI3K-C2α (CPK) selectively binds PtdIns(4,5)P_2 (Song et al., 2001). These observations suggest that a basic residue analogous to Arg58 might be a signature for 3-phosphoinositide binding by PX domains. However, this generalization remains speculative in light of the paucity of PX domains with characterized lipid binding. So far, the CPK PX domain is the single characterized example of a PX domain from the Arg58-lacking subset of PX domains (which also includes PX domains from Bem1p, Bem3p, and Scd2).

Several other interactions with the 3-phosphate appear to help stabilize binding in the pocket: the 3-phosphate also forms hydrogen bonds with the main chain NH groups of Tyr59 and Arg60; the completely conserved Arg105 is also sufficiently close to the 3-phosphate to form a salt link; and helix α2 is oriented so that its helix dipole favorably interacts with the 3-phosphate.

The PX domain of p40^{phox} has great selectivity for PtdIns(3)P over PtdIns(5)P (Ellson et al., 2001b). Modeling a 5-phosphate in the observed position of the 5-hydroxyl indicates that the bulky 5-phosphate would form steric clashes with Arg105 and residues in the PP_{II}/α3 loop. Furthermore, if the PtdIns(5)P headgroup were to bind in a flipped orientation so that the 5-phosphate fit into the same pocket as the 3-phosphate of PtdIns(3)P, critical hydrogen bonds with Arg105 would be lost and small steric clashes in the lipid binding pocket would arise.

The 1-Phosphate Interactions

The nonbridging oxygens of the 1-phosphoryl group make hydrogen bonds with the side chain NZ of Lys92 and NH1 of Arg60. The importance of these interactions is underscored by the results of our mutagenesis. Mutation of Lys92 to Ala greatly decreases the affinity for PtdIns(3)P ($K_d > 50$ μM, Figure 4), and mutation of Arg60 to Ala reduces the affinity by about 3-fold (K_d 18 μM, Figure 4). Although Lys92 is located in the highly variable PP_{II}/α3 loop, it is a strongly conserved residue, which is present in 70% of Pfam PX domains. The proximity of the PP_{II}/α3 loop to the 1-phosphate of the bound phosphoinositide suggests that even in the 30% of PX domains that lack a basic residue equivalent to Lys92, a residue elsewhere in this highly variable loop might assume an analogous role as a 1-phosphate ligand. Although Arg60 is less conserved among PX domains, its importance for PtdIns(3)P binding by p40^{phox} shows that additional residues from other regions may partially contribute to 1-phosphate binding in other PX domains.

The Inositol 4- and 5-Hydroxyl Interactions

The 4- and 5-OH of the inositol moiety form hydrogen bonds with NH1 and NH2 of the conserved Arg105 in helix α3. The essential nature of these interactions is reinforced by the observation that an R105A mutation in the p40^{phox} PX domain eliminates PtdIns(3)P binding (Figure 4) but has no effect on the overall structure as indicated by CD (data not shown). Among PX domains,

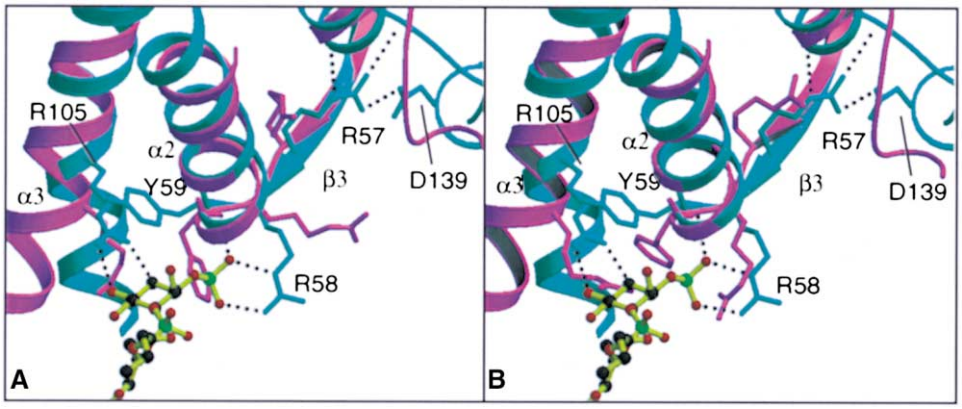

Figure 6. Comparison of the Unliganded p47^{phox} PX Domain with the PtdIns(3)P-bound p40^{phox} PX Domain

(A) A detailed representation of the 3-phosphoinositide binding pocket. The p40^{phox} PX domain ribbon diagram is colored cyan, and the best representative conformer of the p47^{phox} PX domain is colored magenta. The residue numbers refer to the numbering of p40^{phox}. The di-C_4-PtdIns(3)P bound to p40^{phox} is shown in ball-and-stick representation. Most of the structure has been omitted for clarity.

(B) Conformer number 7 of the NMR structure (most similar to the p40^{phox} PX/PtdIns(3)P complex in the binding pocket) is shown superimposed on the p40^{phox} PX structure (representation as in [A]).

this residue is the most conserved basic residue in the phosphoinositide binding pocket. Mutation of the p47^{phox} residue Arg90 (equivalent to p40^{phox} Arg105) dramatically reduced phosphoinositide binding (Kanai et al., 2001), and mutation of the analogous residue in CISK eliminated phosphoinositide binding and endosomal localization (Xu et al., 2001a).

The region around the 4-OH of the p40^{phox} PX domain is well hydrated, raising the question of how the p40^{phox} PX binds selectively to PtdIns(3)P but not to PtdIns(3,4)P_2 (Ellson et al., 2001b; Kanai et al., 2001). This does not appear to be due to lack of a basic residue with which the 4-phosphate could interact: Arg105 appears to be well poised for such a role. However, our molecular modeling of the headgroup binding pocket of the p40^{phox} PX domain suggests that the pocket is too cramped to accommodate a 4-phosphate. The inability of the p40^{phox} PX domain to interact with PtdIns(3,4)P_2 appears to be due to steric constraints at the 4-position caused by the close proximity of Arg105 and other residues in the binding pocket.

Stacking Interactions with the Inositol Ring

One face of the inositol ring (the face with the axial 2-OH) is protected from solvent by the PX domain, most notably by Van der Waals contacts with the side chain of Tyr59. This interaction of an aromatic side chain with a face of the inositide ring is reminiscent of phosphoinositide binding in the catalytic domain of mammalian phosphoinositide-specific phospholipase C (Essen et al., 1996). All of the PX domain members have a Tyr or Phe at the position equivalent to Tyr59 of p40^{phox}, suggesting that this carbohydrate/aromatic stacking is likely to be a common PX domain feature. Mutation of the equivalent residue in the t-SNARE Vam7p and in SNX3 results in a loss of lipid binding and function (Sato et al., 1998; Cheever et al., 2001; Xu et al., 2001b). The importance of aromatic residues stacking against the face of bound sugars is a common feature of carbohydrate recognition by proteins (Duan et al., 2001). The other face of the inositol moiety (opposite the axial 2-OH) is solvent exposed, and the structure shows a collection of water molecules filling the portion of the headgroup binding pocket not occupied by the phosphoinositide (Figure 3). These waters form an extensive network of hydrogen bonds with the hydroxyls of the bound PtdIns(3)P and polar groups on the protein.

Interactions with the Diacylglycerol Moiety

The structure suggests that the p40^{phox} PX domain may form additional interactions with the membrane outside the headgroup binding pocket that may help orient the PX domain on the membrane surface. Tyr94 in the variable loop connecting PP_{II} with α3 makes hydrophobic interactions with the carbons of the glycerol moiety of the bound PtdIns(3)P. Because large chemical shift changes in this region were observed upon micelle binding by the Vam7p PX domain (Cheever et al., 2001), this loop has been termed the "membrane attachment loop" (Wishart et al., 2001). The structures of both p40 and p47 show large, exposed hydrophobic residues in the PP_{II}/α3 loop, suggesting that this may be a common feature among PX domains. Although the Y94A mutant of the p40^{phox} PX domain has only a small influence on binding soluble, monomeric di-C_4-PtdIns(3)P (Figure 4), hydrophobic residues in this loop may have a greater role in binding phosphoinositides in lipid bilayers.

Comparison with the PtdIns(3,4)P_2-Specific p47^{phox} PX Domain

The lipid binding pocket of the p47^{phox} PX domain, which preferentially binds PtdIns(3,4)P_2, is revealed by the NMR structure of the unliganded p47^{phox} PX domain (Hiroaki et al., 2001). One outlying conformer of the bundle of NMR structures, number 7 (PDB entry 1GD5), has a somewhat more open phosphoinositide binding pocket that is more similar to the p40^{phox} PX domain (Figures 3 and 6) and has been used in our comparison of the binding pockets.

The p47^{phox} PX domain has only three basic residues lining the lipid binding pocket (Figure 3). Two of these residues, Arg43 and Lys79, are structurally equivalent

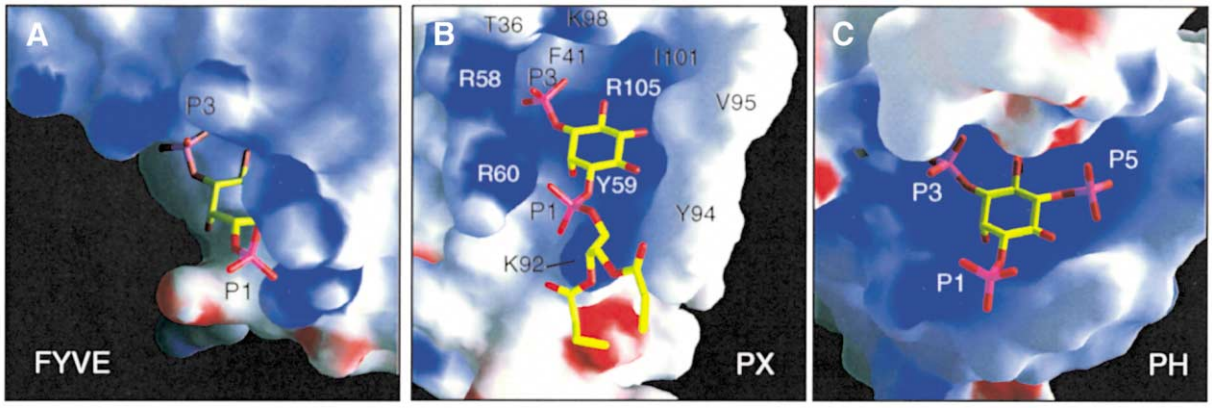

Figure 7. Comparison of Three Phosphoinositide Binding Modules

The phosphoinositide binding sites in the EEA1 FYVE domain (PDB: 1hyi) (Kutateladze and Overduin, 2001), the p40^{phox} PX domain, and the Grp1 PH domain (PDB: 1fgy) (Lietzke et al., 2000) are shown. To illustrate the binding environments, the structures were superimposed using their inositol rings. The molecular surfaces are colored by electrostatic potential.

(A) The EEA1 FYVE domain with PtdIns(3)P bound in a basic pocket.

(B) The p40^{phox} PX domain. The PtdIns(3)P sits in a basic pocket that interacts with one face of the ring, while the other face is exposed to the solvent.

(C) The Grp1 PH domain bound to Ins(1,3,4,5)P_4. As with the p40^{phox} PX domain, only one face of the inositol ring interacts with a basic patch on the surface of the domain.

to the 3-phosphate and 1-phosphate ligands (Arg58 and Lys92) of the p40^{phox} PX domain and presumably assume analogous roles in lipid binding. The third basic residue, Arg90, equivalent to Arg105 in the p40^{phox} PX domain, appears to be the most plausible ligand for the 4-phosphate of PtdIns(3,4)P_2. This suggests that 4-phosphate specificity does not require an additional basic residue. Rather, the shape of the pocket in the vicinity of Arg105, which is dictated principally by residues from helix α3 and the preceding variable PP$_{II}$/α3 loop, seems to determine the specificity. In p40^{phox}, the PP$_{II}$/α3 loop closes off the side of the binding pocket adjacent to the 4- and 5-hydroxyls of the PtdIns(3)P (Figure 3), while the analogous region in p47^{phox} is an open cleft due to a drastically different conformation of the PP$_{II}$/α3 loop. Homology modeling of the CPK PX domain suggests that the conserved basic residue equivalent to Arg105 would be well placed to interact with the 4- and 5-phosphates of PtdIns(4,5)P_2.

Although it is possible to position a PtdIns(3,4)P_2 headgroup in the p47^{phox} lipid binding pocket so that it interacts with the analogous basic residues used by p40^{phox}, the side chain of p47^{phox} Phe44 has a completely different position compared to its p40^{phox} equivalent (Tyr59). For this conserved residue to assume the same role in stacking with the inositol ring, Phe44 and nearby residues would have to undergo a conformational change (Figures 3 and 6). Consistent with this, an NMR study of the Vam7p PX domain shows large chemical shift changes for this residue upon PtdIns(3)P binding (Cheever et al., 2001). The presence of an outlier conformer in the NMR bundle more similar to the PtdIns(3)P-bound conformation even in the absence of PtdIns(3)P may mean that the structure exists in an ensemble of conformations predominated by a "closed" conformation. Phosphoinositide binding might then shift the equilibrium to the "open" members of the ensemble.

The Basic Residue Mutated in CGD Has a Structural, Not a Lipid Binding Role

The residue equivalent to p40^{phox} Arg57 is a highly conserved basic residue among PX domains. Mutation of the analogous residue in the p47^{phox} PX domain (R42Q) is associated with CGD (Noack et al., 2001) and has been shown to eliminate phosphoinositide binding in vitro (Kanai et al., 2001). This and the large chemical shift changes observed on phosphoinositide binding in Vam7p have led to speculation that Arg57 is a phosphate ligand (Cheever et al., 2001). However, the structure of the p40^{phox} PX domain clearly shows that this residue has a very different role in the protein. Although Arg57 is adjacent to the 3-phosphate-interacting Arg58 in the sequence, the side chain of Arg57 is directed away from the PtdIns(3)P binding site (Figures 2, 5, and 6). Instead, Arg57 plays a vital structural role by forming a network of hydrogen bonds that stabilize the unique fold of the PX domain. The side chain NH2 and NE atoms of Arg57 form hydrogen bonds to the main chain carbonyl oxygens of completely conserved, buried Phe132 and of exposed Tyr134, respectively. These hydrogen bonds form a cap at the C terminus of the PX module, enabling the polypeptide to make a sharp kink that passes the residues C-terminal to Tyr134 over the edge of strand β3 and away from the core of the domain. Residues following Tyr134 belong to structural elaborations that are not likely to be common to all PX domains. In addition to terminating helix α4, the Arg57 side chain makes a hydrogen bond with the side chain of Asp 139 and the backbone of Tyr56. The NMR structure of p47^{phox} shows that Arg42 (the equivalent of p40^{phox} Arg57) is also directed away from the phosphoinositide binding pocket and assumes a structural role in the hydrophobic core of the protein. In the NMR conformer more similar to the p40^{phox} PtdIns(3)P-bound conformation, Arg42 makes the same structural interactions with helix α4 as

Table 1. Data Collection, Structure Determination, and Refinement Statistics

Data Collection and MIR Phasing Statistics

Data Set	Resolution (Å)	Observations/ Unique Reflections	Completeness (Last Shell) %	R_{merge}[a]	$\langle I/\sigma \rangle$ (Last Shell)	Number of Sites	Phasing Power[b]	R_{iso}[c]
Native[d]	1.7	55546/18117	89.3 (50.6)	8.5	14.5 (2.5)	—	—	—
$K_3UO_2F_5$[e]	1.9	45224/12747	97.5 (94.7)	9.3	14.0 (1.4)	6	1.65	0.36
K_2PtCl_4[d]	1.9	46900/12717	97.4 (97.4)	8.6	17.5 (1.9)	5	0.69	0.11

Refinement Statistics

Resolution (Å)	Protein Atoms	Heterogen Atoms	Waters	R_{cryst}[f]	R_{free}[f] (% Data Used)	Rmsd from Ideality[g] Bonds	Angles	Dihedrals
30.7–1.7	1150	41	183	0.20	0.23 (5.1)	0.012 Å	1.5°	21.4°

Overall figure of merit 0.41.

[a] $R_{merge} = \Sigma_{hkl}\Sigma_i |I_i(hkl) - \langle I(hkl)\rangle| / \Sigma_{hkl}\Sigma_i I_i(hkl)$.

[b] The phasing power is defined as the ratio of the rms value of the heavy atom structure factor amplitudes to the rms value of the lack-of-cover error.

[c] $R_{iso} = \Sigma ||F_{deriv}| - |F_{native}|| / \Sigma |F_{native}|$.

[d] Both data sets were collected at SRS beamline 9.6. The derivative was soaked in 10 mM K_2PtCl_4 for 30 min.

[e] Soaked in 10 mM $K_3UO_2F_5$ for 1 hr 15 min. Data were collected at SRS beamline 14.1.

[f] R_{cryst} and $R_{free} = \Sigma |F_{obs} - F_{calc}| / \Sigma F_{obs}$; R_{free} calculated with the percentage of the data shown in parentheses.

[g] Rms deviations for bond angles and lengths in regard to Engh & Huber parameters.

seen in p40*phox*, while in the representative conformer, it forms a salt link with Glu46.

The SH3 Domain of p40*phox* Does Not Affect Soluble PtdIns(3)P Binding

Both protein-protein and protein-lipid interactions are critical for activation of NADPH oxidase. In the resting state, the N-terminal SH3 domain from p47*phox* is masked by an intramolecular interaction with a C-terminal region of p47*phox* (Leto et al., 1994; Ago et al., 1999). In the activated complex, the SH3 domain becomes unmasked, leading to an intermolecular interaction with the p22*phox* subunit that is critical for NADPH oxidase activity (Hata et al., 1998). Similarly, it has been proposed that the C-terminal SH3 domain of p47*phox* is masked by an intramolecular interaction with the PP_{II} helix of the PX domain (Hiroaki et al., 2001). The SH3 domain of p47*phox* binds with low affinity ($K_d > 50\ \mu M$) to the p47*phox* PX PP_{II} helix and induces conformational changes in the lipid binding pocket and membrane attachment loop (Hiroaki et al., 2001). In addition, residues within the PXXP motif of Vam7p show large chemical shift changes upon binding PtdIns(3)P and micelles (Cheever et al., 2001). This has led to speculation that SH3 and phosphoinositide binding could affect each other (Cheever et al., 2001; Wishart et al., 2001).

Most PX domains have proline residues analogous to Pro87 and Pro90 in p40*phox*, suggesting that PP_{II} is a rather conserved structural element. However, there are differences in the PX domain proline-rich sequences that can lead to recognition by a specific SH3 domain. For example, the PP_{II} helix of the p47*phox* PX domain binds selectively to the C-terminal SH3 domain of p47*phox* but not to the N-terminal SH3 domain from the same protein nor the SH3 domains from p67*phox* or p40*phox* (Hiroaki et al., 2001). The PP_{II} helix of the liganded p40*phox* PX domain has a fairly different conformation from the unliganded p47*phox* PX domain. The two prolines of the 87-PXXP-90 motif in the p40*phox* PX domain are both buried. This difference between the p40*phox* and p47*phox* PX domains in the conformation of the PP_{II} region may contribute to the specificity of SH3 domain recognition. In previously described structures of proline-rich peptides bound to SH3 domains, at least one proline side chain is exposed to the SH3 domain. If this is a universal requirement for SH3 binding by a proline-rich peptide, it suggests either that the p40*phox* PX domain does not bind an SH3 domain or that there is a conformational change in the PX domain that exposes proline(s) in the absence of bound PtdIns(3)P.

To help clarify the potential role of the SH3 domain in lipid binding by p40*phox*, we compared di-C_4-PtdIns(3)P binding to wild-type, full-length p40*phox* with binding to the full-length protein with a point mutation (W207R) in the SH3 domain (Figure 4). The W207R mutant is analogous to the W263R mutation in the C-terminal SH3 domain of p47*phox* that eliminates SH3 binding by the p47*phox* PX domain (Hiroaki et al., 2001). We find that the mutation has no significant effect on binding soluble lipids, and both constructs bind di-C_4-PtdIns(3)P with a $K_d \sim 3\ \mu M$, an affinity slightly greater than the isolated PX. The single interacting partner that has been identified for the SH3 domain of p40*phox* is a C-terminal region of p47*phox* (Grizot et al., 2001). The effect of the interplay of these interactions on the temporal and spatial activation of NADPH oxidase remains to be elucidated.

Comparison with Other Phosphoinositide Binding Modules

The PX domain has a very different fold from other previously characterized phosphoinositide binding modules, such as FYVE domains (Misra and Hurley, 1999; Driscoll, 2001; Gillooly et al., 2001; Hurley and Meyer, 2001; Kutateladze and Overduin, 2001), PH domains (Ferguson et al., 2000; Lemmon and Ferguson, 2000; Lietzke et al., 2000), and ENTH domains (Ford et al., 2001; Itoh et al., 2001). In contrast to the ENTH domain that binds the PtdIns(4,5)P_2 headgroup at the exposed

tips of the side chains of three basic residues, the FYVE, PX, and PH domains have pockets lined with strategically placed basic residues that embrace the headgroup. Despite their radically different folds, the surface area buried upon lipid headgroup binding is approximately the same for the FYVE, PX, and PH domains (Figure 7). Interestingly, the smallest of these domains, the FYVE domain, is adapted to binding only PtdIns(3)P. In contrast, the PX and PH domain families have members adapted to a broader range of phosphoinositides. FYVE domains bind soluble lipid headgroups with very low affinity (Gaullier et al., 2000; Sankaran et al., 2001) and alone are insufficient for targeting to PtdIns(3)P membranes in vivo (Gillooly et al., 2001). With the single, recently reported exception of FENS-1 (Ellson et al., 2001a; Ridley et al., 2001), FYVE domains require accessory interactions for endosomal localization (e.g., EEA1 requires Rab5). Our results indicate that the p40^{phox} PX domain, like many PH domains, binds readily to soluble phospholipids, and although it is a monomer in solution (Figure 4), it is sufficient for localization to endosomes in vivo.

We have used the PtdIns(3)P-bound p40^{phox} structure along with sequence analysis and experimentally determined binding specificities to understand the headgroup binding preference in structural terms and to suggest rules for predicting phosphoinositide specificity. However, reliably predicting the full range of specificities for the broad family of PX domains will require further studies.

Experimental Procedures

Protein Expression and Purification

The full-length human p40^{phox} (residues 2–339) and the isolated PX domain (residues 2–149) were expressed with an N-terminal MetAlaHis$_6$ tag in *E. coli* strain C41(DE3) at 30°C. The proteins were purified by Ni^{2+} affinity and Heparin sepharose chromatography, followed by gel filtration on a Superdex 75 column (Pharmacia) equilibrated in 10 mM Tris (pH 8.0), 100 mM NaCl, and 2 mM dithiothreitol. The site-specific mutants were created using overlapping PCR and verified by sequencing. Mutants were purified by Ni^{2+} affinity and gel filtration chromatography.

Isothermal Titration Calorimetry

Di-C4-PtdIns(3)P (1 mM) in running buffer (20 mM Tris [pH 7.4] and 100 mM NaCl) was automatically titrated into a 50 μM solution of PX domain or the full-length p40^{phox} in the same buffer, using a MicroCal VP-ITC MicroCalorimeter. Titrations were performed at 20°C, with an injection volume of 6 μl. Data were collected with the VP-ITC control software and analyzed with Origin 50 software (MicroCal). Data were corrected for heats of dilution of PtdIns(3)P into buffer, which were determined in a separate titration.

Crystallization

Crystals were grown by vapor diffusion in hanging drops obtained by mixing 1 μl of a solution containing 8.9 mg/ml protein (in gel filtration buffer) and 2 mM di-C4-PtdIns(3)P (Echelon, P-3004) with 1 μl of a reservoir solution containing 10% PEG 6000, 100 mM HEPES (pH 7.5), 100 mM NaCl, and 15% glycerol. Crystals were propagated by hair seeding, grown at 17°C for 2–3 days, and frozen in a cryoprotectant consisting of 10% PEG 6000, 100 mM HEPES (pH 7.5), 100 mM NaCl, and 25% glycerol.

Data Collection and Structure Determination

Crystals have C2 symmetry with unit-cell dimensions of $a = 96.8$ Å, $b = 33.6$ Å, $c = 76.4$ Å, and $\beta = 132.4°$ and contain one protein molecule in the asymmetric unit. Diffraction data were collected at SRS beamlines 9.6 and 14.1 at 100 K (Table 1). Data were processed using MOSFLM (Leslie, 1992) and CCP4 (CCP4, 1994) programs. Heavy-atom positions were located by autoSHARP (C. Vonrhein et al., personal communication) and refined by SHARP (de La Fortelle and Bricogne, 1997). WARP (Perrakis et al., 1999) was used for initial model building in the SOLOMON (Abrahams and Leslie, 1996) solvent flattened electron density map. Maximum likelihood refinement with CNS (Brünger et al., 1998) was alternated with rounds of manual model rebuilding with O (Jones et al., 1991). The refinement statistics are summarized in Table 1. The structure has 95% of residues in the most favored regions of the Ramachandran plot with no residues in the disallowed regions. No electron density is visible for the residues in the affinity tag or residues 145–149. The density is poorly defined for residues 80–81.

Cellular Localization of the p40^{phox} PX Domain

The wild-type and mutant (R58A) p40^{phox} PX domains (residues 1–149) were cloned into the pEGFP expression vector (Clontech). Constructs were verified by sequence analysis (Babraham Technix).

Porcine aortic endothelial cells (PAEs) were maintained in F12 nutrient mixture (Ham F12, GIBCO-BRL) supplemented with 10% heat-inactivated fetal bovine serum (GIBCO-BRL), at 37°C in a 5% CO_2 humidified atmosphere. PAE cells (1×10^7) were transfected by electroporation with 20 μg total plasmid DNA, as described previously (Stephens et al., 1997). Transfected cells were plated onto glass coverslips and allowed to adhere in complete media for 13 hr prior to serum starvation for 11 hr in F12 media, 0.2% fatty-acid free BSA, 1 U/ml penicillin, and 0.1 mg/ml streptomycin. Cells were fixed in 4% paraformaldhyde, essentially as described previously (Stephens et al., 1997), washed three times in 150 mM Tris (pH 7.4) and once with PBS before being rinsed in water and mounted onto microscope slides with Aqua-polymount antifading solution (Polysciences Inc.). Cells were viewed under a Zeiss Axiphot fluorescent microscope, and images captured using a SPOT digital camera (Diagnostic Instruments).

Analytical Centrifugation

Sedimentation equilibrium analysis was performed in a Beckman Optima XLA analytical ultracentrifuge, using an An-60Ti rotor at 5°C with rotation speeds of either 9,000 or 12,000 rev/min (for the full-length protein and PX domain, respectively). Scans were taken at 280 nm, and data were analyzed as previously described (Cabezon et al., 2000). The best fit to the data was found to be a nonideal single species, in these cases the monomer. Partial specific volumes ($\bar{v}$) and solvent density (ρ) were calculated using the program SEDNTERP (J. Philo on the RASMB software database) and extinction coefficients (ϵ_{280}) calculated with the ProtParam tool. For the p40^{phox} PX domain and full-length p40^{phox}, calculated $\bar{v}$ values were 0.7376 and 0.7314 ml/g, respectively, and the calculated ρ was 1.0044 g/ml.

Acknowledgments

We are grateful to Global Phasing Ltd. for making available the beta-test versions of SHARP and autoSHARP. We thank A. Murzin for helpful discussions, C. Johnson for help with calorimetry, and D. Williams for oligo synthesis. E. Duke and M. Papiz are thanked for help and advice with synchrotron data collection at SRS beamlines 9.6, 14.1, and 14.2. M.P. is supported by a British Marshall Scholarship, C.D.E. by an MRC studentship, K.E.A. by a Beit Memorial fellowship, and P.T.H. by a BBSRC senior fellowship. This work was supported by the Medical Research Council (United Kingdom).

Received July 31, 2001; revised August 6, 2001.

References

Abrahams, J.P., and Leslie, A.G.W. (1996). Methods used in the structure determination of bovine mitochondrial F1 ATPase. Acta Crystallogr. D *52*, 30–42.

Ago, T., Nunoi, H., Ito, T., and Sumimoto, H. (1999). Mechanism for phosphorylation-induced activation of the phagocyte NADPH oxidase protein p47^{phox}. J. Biol. Chem. *274*, 33644–33653.

Arcaro, A., and Wymann, M.P. (1993). Wortmannin is a potent phos-

phatidylinositol 3-kinase inhibitor: the role of phosphatidylinositol 3,4,5-trisphosphate in neutrophil responses. Biochem. J. *296*, 297–301.

Babior, B.M. (1999). NADPH oxidase: an update. Blood *93*, 1464–1476.

Baggiolini, M., Dewald, B., Schnyder, J., Ruch, W., Cooper, P.H., and Payne, T.G. (1987). Inhibition of the phagocytosis-induced respiratory burst by the fungal metabolite wortmannin and some analogs. Exp. Cell Res. *169*, 408–418.

Bateman, A., Birney, E., Durbin, R., Eddy, S.R., Howe, K.L., and Sonnhammer, E.L.L. (2000). The Pfam protein families data base. Nucleic Acids Res. *28*, 263–266.

Brünger, A.T., Adams, P.D., Clore, G.M., DeLano, W.L., Gros, P., Grosse-Kunstleve, R.W., Jiang, J.S., Kuszewski, J., Nilges, M., Pannu, N.S., et al. (1998). Crystallography & NMR system: a new software suite for macromolecular structure determination. Acta Crystallogr. D *54*, 905–921.

Cabezon, E., Butler, P.J.G., Runswick, M.J., and Walker, J.E. (2000). Modulation of the oligomerization state of the bovine F-1- ATPase inhibitor protein, IF1, by pH. J. Biol. Chem. *275*, 25460–25464.

CCP4 (Collaborative Computational Project 4) (1994). The CCP4 Suite: programs for protein crystallography. Acta Crystallogr. D *50*, 760–763.

Cheever, M.L., Sato, T.K., de Beer, T., Kutateladze, T.G., Emr, S.D., and Overduin, M. (2001). Phox domain interaction with PtdIns(3)P targets the Vam7 t-SNARE to vacuole membranes. Nat. Cell Biol. *3*, 613–618.

Cox, D., Tseng, C.-C., Bjekic, G., and Greenberg, S. (1999). A requirement for phosphatidylinositol 3-kinase in pseudopod extension. J. Biol. Chem. *274*, 1240–1247.

de La Fortelle, E., and Bricogne, G. (1997). Maximum-likelihood heavy-atom parameter refinement for multiple isomorphous replacement and multiwavelength anomalous diffraction methods. Methods Enzymol. *276*, 472–494.

Driscoll, P.C. (2001). Solving the FYVE domain-PtdIns(3)P puzzle. Nat. Struct. Biol. *8*, 287–290.

Duan, X., Hall, J.A., Nikaido, H., and Quiocho, F.A. (2001). Crystal structures of the maltodextrin/maltose-binding protein complexed with reduced oligosaccharides: flexibility of tertiary structure and ligand binding. J. Mol. Biol. *306*, 1115–1126.

Ellson, C.D., Anderson, K.E., Morgan, G., Chilvers, E.R., Lipp, P., Stephens, L.R., and Hawkins, P.T. (2001a) Phosphatidylinositol 3-phosphate is generated in phagosomal membranes. Curr. Biol. *11*, 1631–1635.

Ellson, C.D., Gobert-Gosse, S., Anderson, K.E., Davidson, K., Erdjument-Bromage, H., Tempst, P., Thuring, J.W., Cooper, M.A., Lim, Z.-Y., Holmes, A.B., et al. (2001b). PtdIns(3)P regulates the neutrophil oxidase complex by binding to the PX domain of $p40^{phox}$. Nat. Cell Biol. *3*, 679–682.

Esnouf, R.M. (1999). Further additions to MolScript version 1.4, including reading and contouring of electron-density maps. Acta Crystallogr. D *55*, 938–940.

Essen, L.-O., Perisic, O., Cheung, R., Katan, M., and Williams, R.L. (1996). Crystal structure of a mammalian phosphoinositide-specific phospholipase Cδ. Nature *380*, 595–602.

Ferguson, K.M., Kavran, J.M., Sankaran, V.G., Fournier, E., Isakoff, S.J., Skolnik, E.Y., and Lemmon, M.A. (2000). Structural basis for discrimination of 3-phosphoinositides by pleckstrin homology domains. Mol. Cell *6*, 373–384.

Ford, M.G.J., Pearse, B.M.F., Higgins, M.K., Vallis, Y., Owen, D.J., Gibson, A., Hopkins, C.R., Evans, P.R., and McMahon, H.T. (2001). Simultaneous binding of PtdIns(4,5)P_2 and clathrin by AP180 in the nucleation of clathrin lattices on membranes. Science *291*, 1051–1055.

Gaullier, J.M., Ronning, E., Gillooly, D.J., and Stenmark, H. (2000). Interaction of the EEA1 FYVE finger with phosphatidylinositol 3-phosphate and early endosomes. J. Biol. Chem. *275*, 24595–24600.

Gillooly, D.J., Simonsen, A., and Stenmark, H. (2001). Cellular functions of phosphatidylinositol 3-phosphate and FYVE domain proteins. Biochem. J. *355*, 249–258.

Grizot, S., Grandvaux, N., Fieschi, F., Fauré, J., Massenet, C., Andrieu, J.-P., Fuchs, A., Vignais, P.V., Timmins, P.A., Dagher, M.-C., and Pebay-Peyroula, E. (2001). Small angle neutron scattering and gel filtration analyses of neutrophil NADPH oxidase cytosolic factors highlight the role of the C-terminal end of $p47^{phox}$ in the association with $p40^{phox}$. Biochemistry *40*, 3127–3133.

Hata, K., Ito, T., Takeshige, K., and Sumimoto, H. (1998). Anionic Amphiphile-independent Activation of the Phagocyte NADPH Oxidase in a Cell-free System by $p47^{phox}$ and $p67^{phox}$, Both in C Terminally Truncated Forms. J. Biol. Chem. *273*, 4232–4236.

Hiroaki, H., Ago, T., Ito, T., Sumimoto, H., and Kohda, D. (2001). Solution structure of the PX domain, a target of the SH3 domain. Nat. Struct. Biol. *8*, 526–530.

Hurley, J.H., and Meyer, T. (2001). Subcellular targeting by membrane lipids. Curr. Opin. Cell Biol. *13*, 146–152.

Itoh, T., Koshiba, S., Kigawa, T., Kikuchi, A., Yokoyama, S., and Takenawa, T. (2001). Role of the ENTH domain in phosphatidylinositol-4,5-bisphosphate binding and endocytosis. Science *291*, 1047–1051.

Jones, T.A., Zou, J.-Y., Cowan, S.W., and Kjeldgaard, M. (1991). Improved methods for building protein models in electron density maps and the location of errors in these models. Acta Crystallogr. A *47*, 110–119.

Kanai, F., Liu, H., Field, S.J., Akbary, H., Matsuo, T., Brown, G.E., Cantley, L.C., and Yaffe, M.B. (2001). The PX domains of p47phox and p40phox bind to lipid products of PI(3)K. Nat. Cell Biol. *3*, 675–678.

Kraulis, P.J. (1991). MOLSCRIPT: A program to produce both detailed and schematic plots of protein structures. J. Appl. Crystallogr. *24*, 946–950.

Kutateladze, T., and Overduin, M. (2001). Structural mechanism of endosome docking by the FYVE domain. Science *291*, 1793–1796.

Lemmon, M.A., and Ferguson, K.M. (2000). Signal-dependent membrane targeting by pleckstrin homology (PH) domains. Biochem. J. *350*, 1–18.

Leslie, A.G.W. (1992). Recent changes to the MOSFLM package for processing film and image plate data. In Joint CCP4 and ESF-EACMB Newsletter on Protein Crystallography (Daresbury Laboratory, Warrington, UK).

Leto, T.L., Adams, A.G., and de Mendez, I. (1994). Assembly of the phagocyte NADPH oxidase: binding of Src homology 3 domains to proline-rich targets. Proc. Natl. Acad. Sci. USA *91*, 10650–10654.

Lietzke, S.E., Bose, S., Cronin, T., Klarlund, J., Chawla, A., Czech, M.P., and Lambright, D.G. (2000). Structural basis of 3-phosphoinositide recognition by pleckstrin homology domains. Mol. Cell *6*, 385–394.

Marshall, J.G., Booth, J.W., Stambolic, V., Mak, T., Balla, T., Schreiber, A.D., Meyer, T., and Grinstein, S. (2001). Restricted accumulation of phosphatidylinositol 3-kinase products in a plasmalemmal subdomain during Fcγ receptor-mediated phagocytosis. J. Cell Biol. *153*, 1369–1380.

Merritt, E.A., and Bacon, D.J. (1997). Raster3D: Photorealistic molecular graphics. Methods Enzymol. *277*, 505–524.

Misra, S., and Hurley, J.H. (1999). Crystal structure of a phosphatidylinositol 3-phosphate-specific membrane-targeting motif, the FYVE domain of Vps27p. Cell *97*, 657–666.

Nicholls, A., Sharp, K.A., and Honig, B. (1991). Protein folding and association: insights from the interfacial and thermodynamic properties of hydrocarbons. Proteins *11*, 281–296.

Noack, D., Rae, J., Cross, A.R., Ellis, B.A., Newburger, P.E., Curnutte, J.T., and Heyworth, P.G. (2001). Autosomal recessive chronic granulomatous disease caused by defects in *NCF-1*, the gene encoding the phagocyte p47-*phox*: mutations not arising in the *NCF-1* pseudogenes. Blood *97*, 305–311.

Okada, T., Sakuma, L., Fukui, Y., Hazeki, O., and Ui, M. (1994). Blockage of chemotactic peptide-induced stimulation of neutrophils

by wortmannin as a result of selective inhibition of phosphatidylinositol 3-kinase. J. Biol. Chem. *269*, 3563–3567.

Perrakis, A., Morris, R., and Lamzin, V.S. (1999). Automated protein model building combined with iterative structure refinement. Nat. Struct. Biol. *6*, 458–463.

Ponting, C.P. (1996). Novel domains in NADPH oxidase subunits, sorting nexins, and PtdIns 3-kinases: binding partners of SH3 domains? Protein Sci. *5*, 2353–2357.

Prehoda, K.E., and Lim, W.A. (2001). The double life of PX domains. Nat. Struct. Biol. *8*, 570–572.

Ridley, S.H., Ktistakis, N., Davidson, K., Anderson, K.E., Manifava, M., Ellson, C.D., Lipp, P., Bootman, M., Coadwell, J., Nazarian, A., et al. (2001). FENS-1 and DFCP1 are FYVE-domain containing proteins with distinct functions in the endosomal and Golgi compartments. J. Cell Sci., in press.

Sankaran, V.G., Klein, D.E., Sachdeva, M.M., and Lemmon, M.A. (2001). High-affinity binding of a FYVE domain to phosphatidylinositol 3-phosphate requires intact phospholipid but not FYVE domain oligomerization. Biochemistry *40*, 8581–8587.

Sato, T.K., Darsow, T., and Emr, S.D. (1998). Vam7p, a SNAP-25-like molecule, and Vam3p, a syntaxin homolog, function together in yeast vacuolar protein trafficking. Mol. Cell. Biol. *18*, 5308–5319.

Scianimanico, S., Desrosiers, M., Dermine, J.-F., Méresse, S., Descoteaux, A., and Desjardins, M. (1999). Impaired recruitment of the small GTPase rab7 correlates with the inhibition of phagosome maturation by Leishmania donovani promastigotes. Cell. Microbiol. *1*, 19–32.

Segal, A.W., and Abo, A. (1993). The biochemical basis of the NADPH oxidase of phagocytes. TIBS *18*, 43–47.

Simonsen, A., and Stenmark, H. (2001). PX domains: attracted by phosphoinositides. Nat. Cell Biol. *3*, E179–E181.

Song, X., Xu, W., Zhang, A., Huang, G., Liang, X., Virbasius, J.V., Czech, M.P., and Zhou, G.W. (2001). Phox homology domains specifically bind phosphatidylinositol phosphates. Biochemistry *40*, 8940–8944.

Stephens, L.R., Eguinoa, A., Erdjument-Bromage, H., Lui, M., Cooke, F., Coadwell, J., Smrcka, A.S., Thelen, M., Cadwallader, K., Tempst, P., and Hawkins, P.T. (1997). The G$\beta\gamma$ sensitivity of a PI3K is dependent upon a tightly associated adaptor, p101. Cell *89*, 105–114.

Wishart, M.J., Taylor, G.S., and Dixon, J.E. (2001). Phoxy lipids: revealing PX domains as phosphoinositide binding modules. Cell *105*, 817–820.

Xu, J., Liu, D., Gill, G., and Songyang, Z. (2001a). Regulation of cytokine-independent survival kinase (CISK) by the Phox homology domain and phosphoinositides. J. Cell Biol. *154*, 699–705.

Xu, Y., Hortsman, H., Seet, L., Wong, S.H., and Hong, W. (2001b). SNX3 regulates endosomal function through its PX-domain-mediated interaction with PtdIns(3)P. Nat. Cell Biol. *3*, 658–666.

Accession Numbers

The Protein Data Bank code for the structure reported in this article is 1h6h.